



(Ni,Cu)/hexagonal BN nanohybrids – New efficient catalysts for methanol steam reforming and carbon monoxide oxidation

Andrey M. Kovalskii^{a,*}, Andrei T. Matveev^a, Zakhar I. Popov^{a,b,c}, Ilia N. Volkov^a, Ekaterina V. Sukhanova^{a,b,d}, Aleksandra A. Lytkina^e, Andrey B. Yaroslavtsev^{e,f}, Anton S. Konopatsky^a, Denis V. Leybo^a, Andrey V. Bondarev^g, Igor V. Shchetinin^a, Konstantin L. Firestein^h, Dmitry V. Shtansky^a, Dmitri V. Golberg^{h,i,*}

^a National University of Science and Technology "MISIS", Leninskiy prospect 4, Moscow 119049, Russian Federation

^b Emanuel Institute of Biochemical Physics RAS, Kosyginaya 4, Moscow 119991, Russian Federation

^c Plekhanov Russian University of Economics, 36 Stremyannyy per., Moscow 117997, Russian Federation

^d Moscow Institute of Physics and Technology (State University), Institutskiy per. 9, Dolgoprudny, Moscow Region 141701, Russian Federation

^e A.V. Topchiev Institute of Petrochemical Synthesis, Russian Academy of Sciences, Leninskiy prospect 29, Moscow 117912, Russian Federation

^f N.S. Kurnakov Institute of General and Inorganic Chemistry, Russian Academy of Sciences, Leninskiy prospect 31, Moscow 119991, Russian Federation

^g Department of Control Engineering, Faculty of Electrical Engineering, Czech Technical University in Prague, Technicka 2, Prague 6 16627, Czech Republic

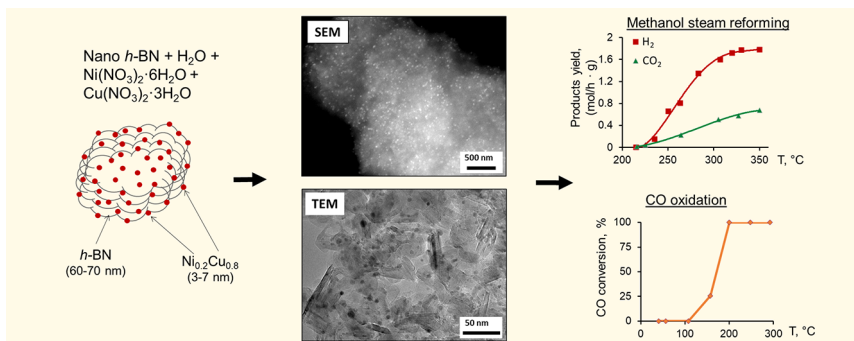
^h Centre for Materials Science and School of Chemistry and Physics, Queensland University of Technology (QUT), 2nd George st., Brisbane, QLD 4000, Australia

ⁱ International Center for Materials Nanoarchitectonics (WPI-MANA), National Institute for Materials Science (NIMS), Tsukuba, Namiki 1, Ibaraki 3050044, Japan

HIGHLIGHTS

- *h*-BN nanosheets as a new promising type of (Ni,Cu) catalyst support.
- (Ni,Cu)/BN nanohybrids demonstrate high catalytic efficiency in methanol steam reforming.
- Nanohybrids exhibit high catalytic stability, selectivity for CO₂.
- Nanohybrids demonstrate high catalytic activity in CO oxidation.

GRAPHICAL ABSTRACT



ARTICLE INFO

Keywords:

Methanol steam reforming
Carbon monoxide oxidation
Catalytic activity
Hexagonal BN
(Ni_{0.2}Cu_{0.8})/BN nanohybrids
Microstructure

ABSTRACT

This work is aimed at the development of bimetallic (Ni_{0.2}Cu_{0.8}) catalysts with hexagonal boron nitride (*h*-BN) nanosheet (BNNS) supports and elucidating their catalytic activity in the methanol steam reforming and CO oxidation reactions. The hybrid Ni_{0.2}Cu_{0.8}/BN catalysts consist of curved *h*-BN nanosheets, up to 10–20 nm in lateral size, decorated with metallic nanoparticles, 3.0–8.2 nm in dimensions. The methanol conversion starts at ~20 °C and is nearly completed at 320 °C. The (Ni_{0.2}Cu_{0.8})/BN nanohybrids exhibit high catalytic stability and high selectivity for CO₂ over the whole temperature range. No carbon monoxide is detected during full methanol conversion. The possible mechanism of CO utilization during methanol reforming is proposed using *ab initio* calculations. The onset temperature of catalytic CO oxidation is 100 °C and full conversion is completed at 200 °C. These results indicate high catalytic efficiency of (Ni_{0.2}Cu_{0.8})/BN nanohybrids in methanol steam reforming and CO oxidation reactions.

* Corresponding authors at: Queensland University of Technology (QUT), 2nd George st., Brisbane, QLD 4000, Australia (D.V. Golberg).

E-mail addresses: a.kovalskii@misis.ru (A.M. Kovalskii), dmitry.golberg@qut.edu.au (D.V. Golberg).

1. Introduction

Active technological developments in recent decades call for solving many pressing problems that humanity faces, in particular, production and conservation of energy and prevention of environmental pollution. Of great interest for future energy is the possibility of converting chemical energy into electrical energy utilizing fuel cells and using proton exchange membranes [1,2]. In the past, special attention has been paid to the development of methods for producing hydrogen from natural gas and alcohols obtained from a biomass [2–5]. However, until now, there has been no hydrogen production technology which is entirely ecologically safe and the main current goal is to reduce environmental risks while simplifying hydrogen production. Using methane as a feedstock seems to be an advantageous pathway, but the peculiarities of its conversion at a high temperature make this process complex and expensive [6–14]. Due to alcohols high chemical activity, their steam reforming occurs at much lower temperatures [15–17]. Therefore, the number of studies devoted to the hydrogen production is rapidly increasing [18].

The development of an effective methanol dehydrogenation catalyst with high activity, selectivity and stability is an extremely important task, as it would allow one to safely obtain hydrogen and to reduce an environmental risk [19]. To increase the activity of such catalyst it is effective to increase its dispersion and specific surface area of its support [20]. Variation of catalyst material composition using bimetallic alloys, which serve as the main reaction promoters and inhibitors, greatly contributes to catalyst selectivity improvement.

Reduction of catalyst activity can occur for several reasons, such as agglomeration, sintering of active metal particles and contamination of catalyst and/or support surface during the interaction with a working fluid. The catalysts based on Cu, Ni, Co, Fe, Pd, Pt, Ru, Ir, Ag, and Au are often used in methanol steam reforming. However, it has been shown that the activity of metal catalysts can be improved by introducing another metal as an additive. For example, the addition of Ni to Cu significantly increases Cu stability in reaction of methanol steam reforming [21]. The most common catalyst supports are TiO₂ [22], ZrO₂ [21,23,24], γ-Al₂O₃ [25,26], ZnLaAlO₄ [25], CeO₂ [27], SiO₂ [28–30], detonated nanodiamonds (DND) [31] and others. The complete conversion of hydrogen to (Ni,Cu) catalyst takes place in a temperature range of 300–400 °C. The lowest conversion temperature was observed for catalysts onto TiO₂ supports [22]. The use of membrane catalysis improves the reforming efficiency and make possible the obtaining of pure hydrogen suitable for use in fuel cells [6,18,32].

Carbon monoxide (CO) oxidation is another industrially important catalytic reaction that can be employed for purification of hydrogen-rich gases, emission control, and air purification [33,34]. CO gas is toxic and should not be released into the environment. The catalysts used to convert CO to CO₂ are expected to possess high CO oxidation activity, selectivity, and decent resistance toward deactivation by H₂O and CO₂ [35]. Due to ability to dissociate molecular oxygen at relatively low temperatures and bind strongly with both atomic oxygen and CO, transition metals, such as Pt, Pd, Rh, Ru, Ag, and Au, are considered as the most effective catalysts. To reduce the cost of noble metals and further improve catalytic performance, other metals, such as Ni, Cu, Co, Fe and their combinations have been in the focus of recent studies [36,37].

Hexagonal boron nitride (*h*-BN) is considered as a new and effective catalyst support. It should be noted that despite the large number of theoretical works directly or indirectly related to the catalytic properties of *h*-BN nanoparticles, experimental studies on this topic are rather scarce. As has previously been reported [38], *h*-BN reveals its own catalytic activity due to oxygen-terminated arm-chair BN edges that act as catalytic active sites. Since *h*-BN has a high oxidation resistance, it is difficult to form B-O species at the arm-chair edges during oxidative dehydrogenation, which usually occurs below 600 °C. To overcome this shortcoming, C-H activation to form B-O(H) active sites has been

proposed [39]. Catalytically active elements (Pt, Ag) on *h*-BN supports often exhibit increased catalytic activity compared to widespread Al₂O₃ and CeO₂ supports [40,41]. In addition, as a result of redistribution of electron density on BN, defect-free *h*-BN surface possesses catalytic activity under interactions with metal nanoparticles [42,43].

Several methods for catalyst production should be mentioned. These involve deposition, impregnation, autoclaving, and reverse refrigeration. The choice of a method depends on the nature of the catalyst itself and/or the physical-chemical characteristics of the support. The most commonly used approach for metal catalysts production is the impregnation method. The use of such method is very difficult for an *h*-BN as a support, since *h*-BN is typically hydrophobic and it is problematic to impregnate it with a solution [44]. It has been reported, however, that metal atoms bind directly to *h*-BN defects, which act as trapping sites for them [45]. Therefore wet chemistry method requires optimization and/or modernization. The aim of this work is the development of bimetallic (Ni,Cu)/BN catalysts on the new type of support - *h*-BN nanosheets (BNNSSs) - and elucidation of their catalytic activity in the methanol steam reforming and CO oxidation reactions.

2. Experimental

2.1. Synthesis of BN nanoparticles

Boron oxide (BO)-assisted chemical vapor deposition (CVD) process was used for the synthesis of BNNSSs using a vertical CVD furnace with an induction heating system operating at 41.4 kHz. The experimental set-up was described elsewhere [46]. To remove impurities (boron oxide and hydroxide) formed on the surface of BNNPs during the CVD, the synthesized products were sonicated in distilled water for 2 h, rinsed in distilled water five times, and centrifuged. Then BNNPs were annealed in vacuum at 1500 °C for 1 h.

2.2. Synthesis of (Ni,Cu)/BN nanohybrids

As has experimentally been shown using a ZrO₂ support, among different (Ni,Cu) compositions the most active and selective catalyst for methanol steam reforming is (Ni_{0.2}Cu_{0.8}) [20]. Therefore, this composition was chosen to produce catalyst nanoparticles on the BNNSSs as a new type of (Ni,Cu) catalyst support for the methanol steam reforming and CO oxidation reactions.

To obtain (Ni,Cu)/BN catalysts, the BN powder was impregnated by using a classical wet chemistry process. BN particles were sequentially impregnated with aqueous solutions of Ni(NO₃)₂·6H₂O (pure) and Cu (NO₃)₂·3H₂O (99%, Acros Organics). The amount of nitrates was calculated for a metal content equal to 20 wt% of the BN support. 250 mg of BNNSSs with Ni and Cu nitrates taken in the required quantities were firstly dispersed in a distilled water with an addition of 3–5 wt% ethanol using an ultrasonic bath for 2 h to destroy agglomerates. Such processing leads to partial *h*-BN nanoparticle hydrolysis, which could contribute to the formation of functional groups and surface defects. Then excess of water was evaporated at 120 °C under constant stirring. The obtained residue after evaporation in an alumina boat was kept at 350 °C in vacuum for 1 h and then treated at 350 °C for 3 h under hydrogen (15 cm³/min) and argon (80 cm³/min) flows in a tube furnace. As a result the bimetallic (Ni_{0.2}Cu_{0.8})/BN catalysts were obtained. Among earth-abundant transition metals, Ni and Cu have the smallest lattice mismatch (< 2.3%) with *h*-BN, which can facilitate their nucleation on the *h*-BN surface.

2.3. Catalytic tests

2.3.1. Methanol steam reforming

Methanol steam reforming was carried out at atmospheric pressure using a flow-type installation in the stainless steel tubular reactor in the temperature range of 200–400 °C. The installation scheme is shown in

Fig. 1. Catalyst powder was mixed with granulated quartz of 1–3 mm fraction and placed into the reactor. The mass of BN support with the catalyst for experiments on steam reforming of methanol was 300 mg. Heating of the catalyst in the reactor was carried out in a resistance electric furnace in an argon flow of 20 cm³/min. Temperature of reactor was controlled by a chromel-alumel thermocouple. Catalyst was reduced *in situ* at a temperature of 350 °C with a mixture of H₂ (1 cm³/min) and Ar (20 cm³/min) for 3 h before every experiment. During the reaction, argon flow rate was constant and equaled to 20 cm³/min. A mixture of methyl alcohol with distilled water, taken in a 1:1 M ratio was fed through an evaporator by an infusion pump Instilar 1488 Dixion with a rate of 1.5 cm³/h. Unreacted alcohol and water were condensed in a cooled to +1 °C glass collector. Analysis of uncondensed reaction products was performed by a gas chromatograph LHM 8MD operated with a thermal conductivity detector with helium as a carrier gas, and columns with stationary phases Porapak T for water, methanol and other oxygenates, and activated carbon for CO and CO₂. Concentrations of hydrogen and methane in products were measured by a chromatograph Chrom-4 with a thermal conductivity detector and a zeolite CaA Zeosorb column, with Ar as a carrier gas.

2.3.2. Carbon monoxide oxidation

Controlled CO oxidation reaction was performed on a ChemBET Pulsar instrument (Quantachrome). Catalytic performance of the (Ni_{0.2}Cu_{0.8})/BN nanohybrids was analyzed using CO oxidation in a fixed-bed continuous-flow reactor at the ambient pressure. 50 mg of the catalyst diluted with quartz granules was placed into a quartz U-tube with a 4 mm inner diameter. Catalyst activation was conducted in a gas flow of 10% H₂/90% He with a total flow rate of 36 ml/min at 350 °C for 1 h. The activity measurements were carried out in a gaseous mixture of 5.6 mol.% of CO, 11.1 mol.% of O₂, and 83.3 mol.% of He under a total flow rate of 36 ml/min (GHSV = 43200 ml·g_{cat}⁻¹·h⁻¹). Analysis of the catalytic reaction products was performed using a quadrupole mass spectrometer Thermostar GSD 320 (Pfeiffer Vacuum). The CO conversion was calculated according to the following equation:

$$\alpha = 1 - \frac{f_{CO}^{out}}{f_{CO}^{in}}$$

where f_{CO}^{out} is a CO gas flow rate after the catalyst bed and f_{CO}^{in} is an initial CO gas flow rate.

2.4. Material characterization

The synthesized product morphologies and compositions were analyzed using a scanning electron microscope JSM-7600F (JEOL) equipped with an energy-dispersive X-ray (EDX) detector. The microstructure of samples was examined by means of transmission (TEM) and scanning transmission electron microscopy (STEM) using a 200 kV JEM-2100 instrument (JEOL). The powder samples for TEM were ground in methanol, and the resulting dispersion was transferred to a holey carbon film deposited on the Cu supported grid.

Chemical and phase compositions were investigated by EDX spectroscopy using a 80 mm² X-Max EDX detector (Oxford Instruments), X-ray diffraction (XRD) analysis using a DRON-3 diffractometer

(Burevestnik) operated with Co K α radiation, and Fourier-transform infrared spectroscopy (FTIR) with a Vertex 70v vacuum spectrometer (Bruker) in the range of 400–2000 cm⁻¹ using the partial internal reflection device.

The concentration of Ni and Cu ions in catalysts was studied by means of inductively coupled plasma mass spectrometry (ICP-MS) using an X-Series II unit (Thermo Fisher Scientific). To prepare a sample for measurement, 15 mg of catalyst powder was dissolved in a mixture of concentrated acids (1 ml HNO₃ + 3 ml HCl + 1 ml HF) and kept in the microwave at 220 °C for 20 min. Then the solution was adjusted to 50 ml and finally diluted 50 times.

Chemical composition of sample surfaces was analyzed by X-ray photoelectron spectroscopy (XPS) using an Axis Supra spectrometer (Kratos Analytical). The maximum lateral dimension of the analyzed area was 0.7 mm. The spectra were fitted using CasaXPS software after subtracting Shirley-type background. The BEs for all environments were employed from the literature [47–50].

2.5. Theoretical modeling

In order to investigate the adsorption process, quantum-mechanical calculations were performed using density functional theory (DFT) [51,52] implemented in VASP program package within the Perdew, Burke and Ernzerhof (PBE) [53] exchange-correlation functional. The electronic wave functions were described using the projector augmented wave (PAW) potential [54] with the energy cutoff of 450 eV. The k -point meshes were generated by Monkhorst-Pack scheme for integration over the first Brillouin zone [55]. The structural relaxations were made until the energy difference between two optimization steps became less than 10⁻³ eV. The DFT-D3 corrections [56] were used to take into account the van der Waals interactions between material layers. In order to avoid interactions between periodic images of the adjacent cells and between gas molecules, the vacuum length was chosen equal to 12 Å and 5 × 5 × 1 supercells of Ni, Cu and h-BN were considered. The Brillouin zone sampling was made with a 2 × 2 × 1 k -point mesh.

3. Results

3.1. Structural characterization

FTIR spectra of as-synthesized material (before and after purification) are shown in Fig. 2a. The FTIR spectrum recorded from the particles after the synthesis reveals two characteristic main features – broad bands at 794 and 1375 cm⁻¹, corresponding to out-of-plane B-N-B bending and in-plane B-N stretching vibrations, respectively [57]. Similar spectrum recorded from the same particles after the subsequent purification also exhibits two sharp peaks at 808 and 1377 cm⁻¹. These peaks are the fingerprints of a sp²-bonded BN. First spectrum (as-synthesized BN) has some additional features such as broad zones with a high absorbance in the ranges of 400–720, 850–1200, and 3000–3500 cm⁻¹. These features can be due to some amount of oxygen and/or O-H impurities [57,58], which are apparently related to the BO-assisted CVD synthesis of the material. Spectrum recorded from

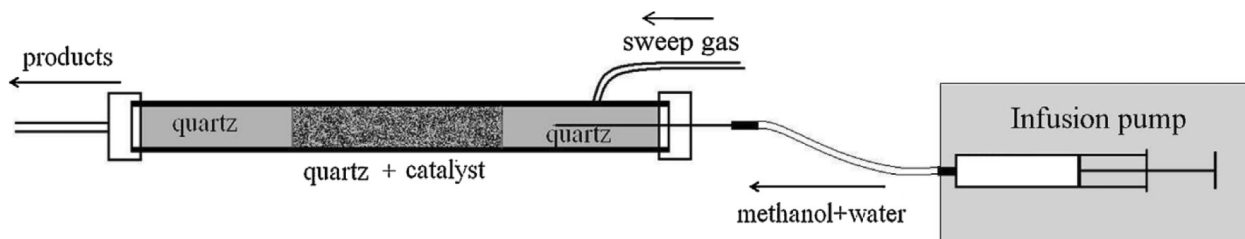


Fig. 1. Scheme of the reactor with a stationary catalyst layer for study of methanol steam reforming.

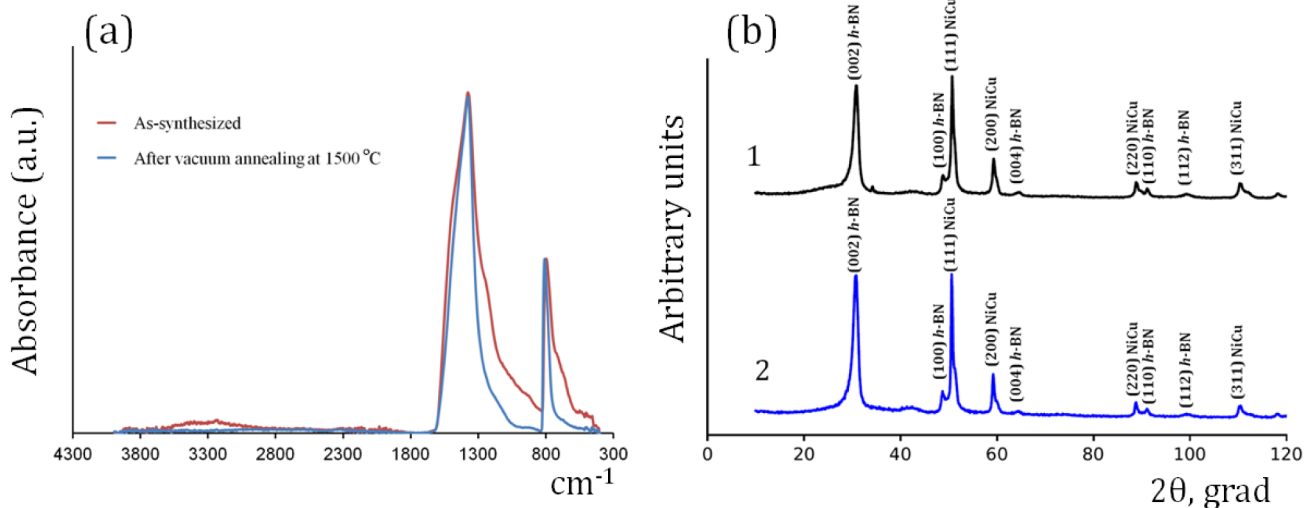


Fig. 2. FTIR spectra of BNNPs before and after high-temperature annealing in vacuum (a) and XRD patterns of ($\text{Ni}_{0.2}\text{Cu}_{0.8}$)/BN nanohybrids (b) before (1) and after (2) catalytic tests.

particles after the purification is free from additional peaks responsible for oxygen and O–H impurities, thereby confirming the effectiveness of the purification process.

Fig. 2b shows the XRD pattern (1) of the ($\text{Ni}_{0.2}\text{Cu}_{0.8}$) catalyst supported onto BNNSs. The XRD pattern reveals characteristic peaks from the *h*-BN phase and $\text{Ni}_{0.2}\text{Cu}_{0.8}$ alloy. The (1 1 1) interplanar distance (0.206 nm) of $\text{Ni}_{0.2}\text{Cu}_{0.8}$ is just between the values for the pure Cu (0.208 nm) and Ni (0.204 nm) metals.

The results of EDX spectroscopy analysis indicated that the B/N atomic ratio in the BNNSs is close to 1:1 and the content of oxygen impurities is low. The EDX spectroscopy investigation of annealed BNNSs showed a decrease in the proportion of the boron-oxide phase.

XPS analysis (Fig. 3a,d) revealed that the pristine BN nanostructures are mainly composed of boron and nitrogen, although some traces of oxygen were also detected (Table 1). As documented by B1s curve fitting, the concentrations of boron oxynitride (BNO) and boron suboxide (BO_x) are very low (Fig. 3a and Table 2). The high quality of BN powder was also confirmed by N1s curve fitting, revealing that ~80% of nitrogen signal comes from the BN phase (Fig. 3d). The data is summarized in Tables 2 and 3.

Thus, XRD, FTIR, XPS, and EDX spectroscopy analyses evidenced that the synthesized and then annealed material is a powder of BNNSs with a B/N ratio close to the stoichiometric one. This material was then used for fabrication of ($\text{Ni}_{0.2}\text{Cu}_{0.8}$)/BN hybrid catalysts.

According to the SEM data, the synthesized hybrid catalysts consist of BNNS agglomerates with metal nanoparticles (NPs) uniformly distributed over their surfaces (Fig. 4a). Only the largest metal NPs, 10–25 nm in size, are observed by SEM. EDX spectroscopy analysis of the area of the catalyst material shows that the content of the metal phase is in the range of 1–1.5 at.% with the Cu/Ni ratio equal to 4–5:1.

TEM data provides the detailed information on the morphology and structure of ($\text{Ni}_{0.2}\text{Cu}_{0.8}$)/BN nanohybrids. On the bright-field TEM image of nanohybrids (before the reaction of methanol steam reforming), curved sheets of *h*-BN, 10–20 nm in lateral size, are clearly visible (Fig. 5a). Dark isometric NPs of metal phase are located on the surface of BN phase. The size of metal NPs before methanol steam reforming changes within the range of 3–8 nm. The high-resolution TEM micrograph presented in Fig. 5b reveals metal NP located on the surface of a BN nanosheet. The observed interplanar distances are in a good agreement with $\text{Ni}_{0.2}\text{Cu}_{0.8}$ and *h*-BN phases. $\text{Ni}_{0.2}\text{Cu}_{0.8}$ NP size distribution is shown in Fig. 5c. The majority of metal NPs is approximately 4.5 nm in size and more than 90% of them are less than 6.5 nm. Statistical TEM image processing showed that, on average, 60–80 small

NPs (< 8.2 nm) are found within the area of 10^4 nm^2 , although single NPs, up to 25 nm in size, may also exist (Fig. 4a).

The concentration of Cu and Ni in the ($\text{Ni}_{0.2}\text{Cu}_{0.8}$)/BN catalysts was determined by EDX spectroscopy, ICP-MS, and XPS methods. According to the EDX spectroscopy analysis, the Ni/Cu ratio in the ($\text{Ni}_{0.2}\text{Cu}_{0.8}$)/BN nanohybrids was close to 1:4. About 1.2 and 5.5 wt% of Ni and Cu were measured by ICP-MS method indicating a ratio of Ni/Cu = 1:4.6. Cu content of 0.51 at. % was detected on the surface of ($\text{Ni}_{0.2}\text{Cu}_{0.8}$)/BN catalyst by XPS. Based on the Ni/Cu ratio reported above, the concentration of Ni on the sample surface should be as small as ~0.1 at.%. This value is below the XPS detection limit for this particular element.

The B1s and N1s curve fitting revealed that the growth of metal NPs on the BN nanostructures had not affected the BN structure, i.e. the concentrations of B and N environments remain in the same range (within error margins), as shown in Fig. 3b and 3e and in Tables 2 and 3. The Cu 2p3/2 curve fitting revealed that metal NPs are composed of copper (Cu^0), copper oxide (CuO) and $\text{Cu}(\text{OH})_2$. The Cu 2p3/2 curve fitting is shown in Fig. 6a and the Cu environment fractions are presented in Table 4. The Cu^0 peak position at 932.9 eV is typical for the $\text{Ni}_x\text{Cu}_{1-x}$ particles [59,60] being in a good agreement with our results. The BE value for bulk Cu is $932.6 \pm 0.2 \text{ eV}$ [61], but, in case of nanoparticles, the peak position can be shifted due to a size effect [62]. The contribution from CuCO_3 (~935 eV [61]) cannot be entirely excluded.

3.2. Catalytic activity in methanol steam reforming

Fig. 7a shows the temperature dependence of the reaction product yields while using the ($\text{Ni}_{0.2}\text{Cu}_{0.8}$)/BN catalyst (red curve). The reaction starts at about 220 °C and nearly full conversion accomplishes at 320 °C. Thus, the catalyst shows excellent results with respect to hydrogen yield. The catalytic stability of the ($\text{Ni}_{0.2}\text{Cu}_{0.8}$)/BN nanohybrids is demonstrated in Fig. 7a (inset). The ($\text{Ni}_{0.2}\text{Cu}_{0.8}$)/BN catalyst keeps its high H_2 conversion rate during 15 h at 315 °C, suggesting its high catalytic stability. The yield of carbon dioxide is kept low throughout the whole temperature range up to full conversion of methanol (Fig. 7b). It is important to note that no CO is observed for all reaction products.

3.3. Structural characterization after methanol steam reforming

The XRD patterns of the ($\text{Ni}_{0.2}\text{Cu}_{0.8}$)/BN nanohybrids before and after catalytic test are similar (Fig. 2b) indicating that heating to 350 °C

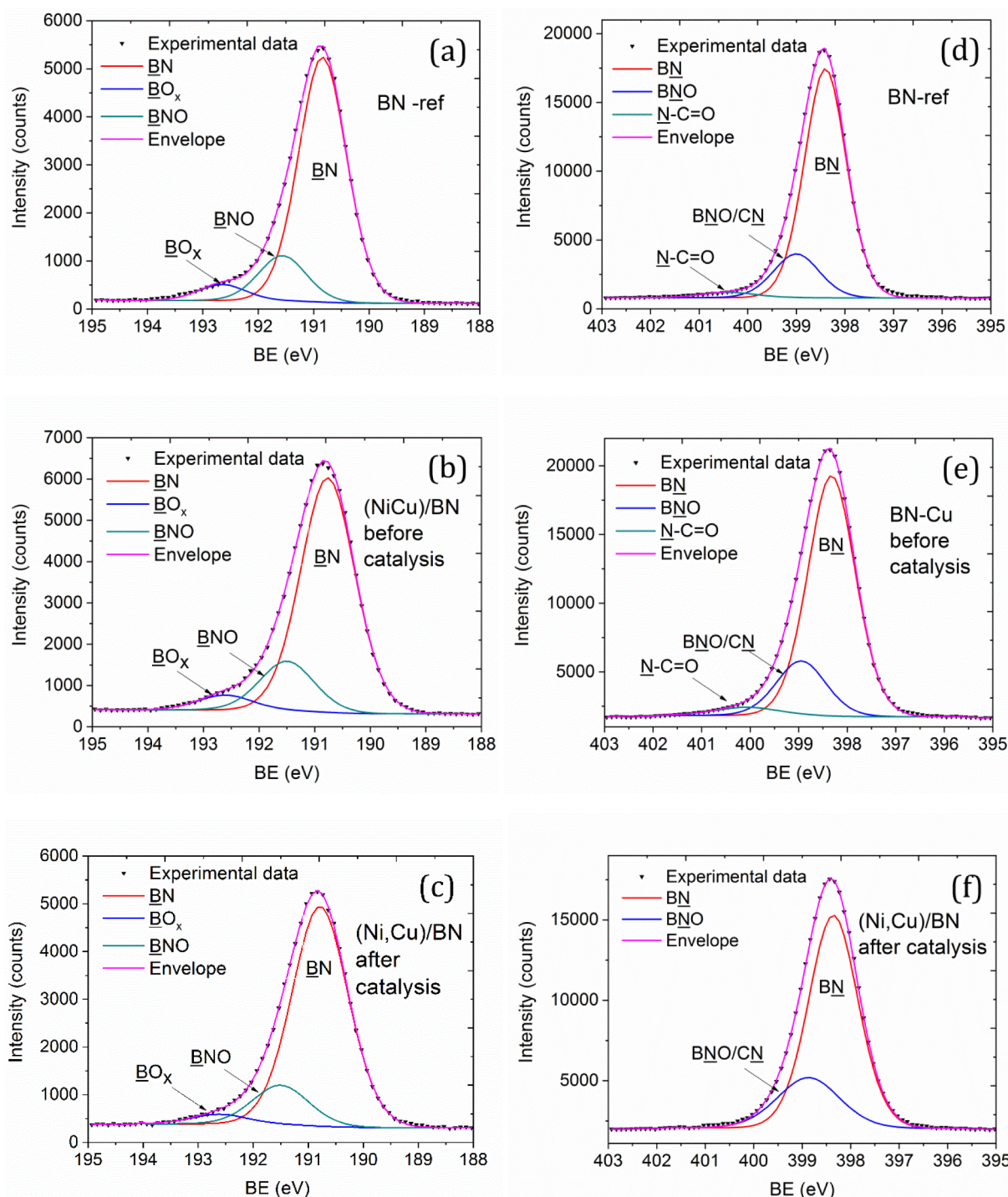


Fig. 3. XPS B1s (a-c) and N1s (d-f) spectra and their curve fitting. BN-ref (a,d), ($\text{Ni}_{0.2}\text{Cu}_{0.8}$)/BN nanohybrids before (b,e) and after (c,f) catalytic tests.

Table 1

Elemental composition (at.%) of the samples derived from XPS measurements.

Sample	B	N	O	Cu	Cu/B
BN-ref	43.3	46.8	9.9	0.00	0
($\text{Ni}_{0.2}\text{Cu}_{0.8}$)/BN before catalysis	41.3	43.0	15.2	0.51	0.012
($\text{Ni}_{0.2}\text{Cu}_{0.8}$)/BN after catalysis	38.6	39.5	21.3	0.62	0.016

has not changed the phase composition. Although most of the metallic NPs have kept their size below 10 nm (Fig. 5d), larger NPs, reaching the size of 50 nm are also visible in the corresponding SEM image (Fig. 4b). EDX spectroscopy profile (Fig. 5f) of the metal NPs presented in Fig. 5e indicates that their composition is close to $\text{Ni}_{0.2}\text{Cu}_{0.8}$.

Interestingly, the ($\text{Ni}_{0.2}\text{Cu}_{0.8}$)/BN samples after catalytic tests demonstrated very similar Cu contents, i.e. no Cu loss was detected by XPS (Fig. 6b). However, some differences in the samples surface composition were determined. Although the Cu 2p3/2 signal was fitted with the same three peaks as for BN-Cu before catalysis, the fractions of various Cu environments were different. The metallic Cu fraction Cu^0

Table 2

Fractions (%) of different boron environments derived from XPS B1s curve fitting.

Sample	<u>BN</u> (BE = 190.8 eV, FWHM = 1.2 ± 0.05 eV)	<u>BNO</u> (BE = 191.5 eV, FWHM = 1.2 ± 0.05 eV)	<u>BO_x</u> (BE = 192.6 eV, FWHM = 1.2 ± 0.05 eV)
BN-ref	80.0	14.8	5.2
(Ni _{0.2} Cu _{0.8})/BN before catalysis	78.4	16.6	5.0
(Ni _{0.2} Cu _{0.8})/BN after catalysis	81.8	14.7	3.6

was increased by 8.6% at the expense of CuO and Cu(OH)₂ components (Fig. 6b and Table 4). Nitrogen environment of (Ni_{0.2}Cu_{0.8})/BN after catalysis exhibited no more N-C=O contribution (Fig. 3f). The boron environment demonstrated no changes (Fig. 3c).

3.4. Catalytic activity in CO oxidation

The results of catalytic activity tests using the pre-activated at 350 °C (Ni_{0.2}Cu_{0.8})/BN nanohybrids in the reaction of CO oxidation are presented in Fig. 8. The onset temperature of catalytic CO oxidation is 100 °C and a full conversion is observed at 200 °C. This result is comparable with Ag/BN nanocatalysts (1.36 wt% of Ag) for which the full conversion temperature was 194 °C [63]. Interestingly, the obtained results may explain the absence of CO during methanol steam reforming reaction. The CO oxidation is completed at 200 °C, whereas the onset temperature of methanol reforming is 220 °C. This means that above 220 °C all carbon monoxide, which can be related product during methanol reforming, should almost immediately oxidize.

4. Discussion

4.1. (Ni_{0.2}Cu_{0.8})/BN catalysts in the reaction of methanol steam reforming

There have been many studies on Cu-containing catalysts for the reaction of methanol steam reforming. To evaluate the efficiency of the obtained catalyst, as well as the possible effect of nano-BN supports, a comparison to similar catalysts with other ceramic supports was made. In Fig. 7a,b the temperature dependences of the H₂ and CO₂ yields in the methanol steam reforming reaction using catalysts with the same concentration of Ni_{0.2}Cu_{0.8} particles, but on different supports: e.g. DND [31] and ZrO₂ [24], are compared with the present (Ni_{0.2}Cu_{0.8})/BN catalyst. Although, the starting temperature of H₂ yield for Ni_{0.2}Cu_{0.8} catalysts supported with DND and ZrO₂ was 20 °C lower than in our experiments, the H₂ yield in the range of 200–220 °C was also very low (< 10%). Among the three materials compared, the catalysts based on ZrO₂ (annealed at 350 °C) [24] and BN (this work) supports show a significantly higher activity, as compared with (Ni,Cu)/DND catalyst [31]. Fig. 7b compares the temperature dependence of CO₂ yield in methanol steam reforming reaction on (Ni_{0.2}Cu_{0.8})/BN and (Ni_{0.2}Cu_{0.8})/ZrO₂ catalysts. Although these catalysts slightly differ with respect to temperatures of the beginning and end of the reaction, the amount of CO₂ formed was approximately the same (0.7 mol/h·g). The CO flow in methanol steam reforming reaction using (Ni_{0.2}Cu_{0.8})/DND and (Ni_{0.2}Cu_{0.8})/ZrO₂ catalysts reached 0.012 and 0.002 mol/h·g, respectively at 320–330 °C (Fig. 7c), whereas in our experiments CO was not detected at all. Thus the (Ni_{0.2}Cu_{0.8})/BN catalyst exhibits high selectivity for CO₂ over the whole temperature range. Since carbon oxide

impurities are undesirable by-products in the reaction of methanol steam reforming, (Ni,Cu)/BN nanohybrids should be placed among the most effective catalytic systems.

4.2. Methanol reforming mechanism

The absence of CO and other intermediate products during methanol steam reforming [64–68] suggests that, in our case, the steam reforming proceeds through the following reaction:



In a number of studies, the production of hydrogen was proposed to be accomplished via an initial methanol decomposition reaction followed by a water gas shift reaction [69]:



The high activity of the (Ni_{0.2}Cu_{0.8})/BN catalyst in the catalytic oxidation of CO suggests that if the reactions (2) and (3) take place, the carbon monoxide should almost instantly oxidize. To confirm this assumption further, we carried out the theoretical calculations presented below.

4.3. Theoretical modeling

The early theoretical modelling of the CO oxidation mechanisms in h-BN/Ni [70] and on h-BN/Cu [71] heterostructures showed a small oxidation barrier of 0.51 eV during the interaction of CO with pre-dissociating O₂ molecule adsorbed on the h-BN/metal heterostructure. In order to explain the absence of CO gas in the steam products in our catalytic tests, the possible mechanism of CO utilization during methanol reforming was proposed using *ab initio* calculations. In our theoretical model the (Ni,Cu)/BN hybrid was considered as a NiCu_x/h-BN heterostructure in which nitrogen atoms are located above metal atoms (top site), while boron atoms are placed at the hollow site of the face-centered cubic (fcc) metal structure. The fcc configuration was selected because it is the most energetically favorable one [72,73]. Besides NiCu₄, the metal Ni and Cu surfaces were also considered for comparison. Metal and h-BN cell parameter mismatches were 3.9, 1.0, and 1.8% for Ni(1 1 1), Cu(1 1 1) and NiCu₄(1 1 1), respectively. The distances between the h-BN monolayer and the metal layer were considered in calculation as 2.10, 3.09, and 2.89 Å for Ni, Cu, and NiCu₄, respectively. The optimized distances for Cu and Ni are in a good agreement with previously published data [74] and for Cu₄Ni, the distance is just between the two values, which confirm the correctness of the selected model. The interaction between Cu₄Ni surface and h-BN

Table 3

Fractions (%) of different nitrogen environments derived from XPS N1s curve fitting.

Sample	<u>BN</u> (BE = 398.4 eV, FWHM = 1.1 ± 0.05 eV)	<u>BNO</u> (BE = 399.0 eV, FWHM = 1.2 ± 0.05 eV)	<u>N-C=O</u> (BE = 400.4 eV, FWHM = 1.4 ± 0.1 eV)
BN-ref	80.7	16.9	2.4
(Ni _{0.2} Cu _{0.8})/BN before catalysis	78.0	18.5	3.5
(Ni _{0.2} Cu _{0.8})/BN after catalysis	77.2	22.8	0.0

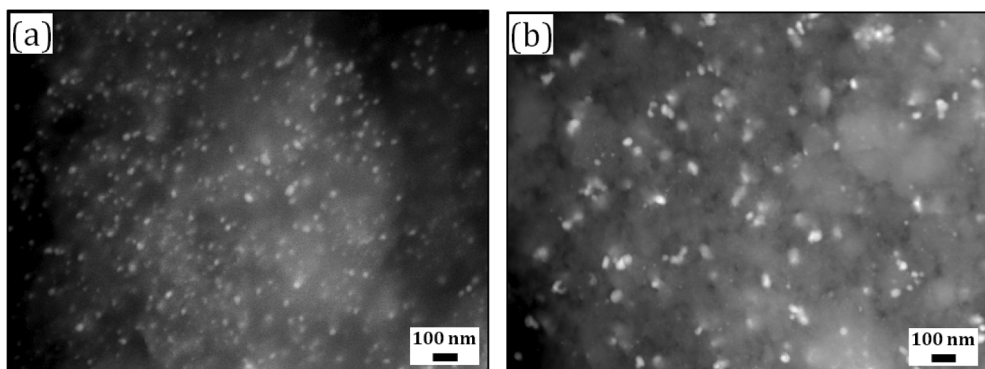


Fig. 4. SEM images of $(\text{Ni}_{0.2}\text{Cu}_{0.8})/\text{BN}$ nanohybrids before (a) and after (b) catalytic tests.

plane leads to the electron transfer toward *h*-BN due to electronegativity difference and charge redistribution in the *h*-BN plane (Fig. 9a). Partial-support interaction has previously been studied for Ni/*h*-BN and Cu/*h*-BN systems. Strong orbital hybridization between Ni 3d and *h*-BN π states is observed, suggesting a rather strong interfacial interaction between *h*-BN and Ni substrate [75]. In contrast, Cu 3d-*h*-BN π hybridization is much weaker and the *h*-BN monolayer is only

weakly chemisorbed [76]. According to DFT calculations, the binding energy (BE) *per* BN unit for *h*-BN/Ni and *h*-BN/Cu is -0.25 and -0.16 eV, respectively [74]. For different 3d, 4d, and 5d transition metals the N atom was shown to repel from the metal surface, whereas the B atom is attracted to it [72]. The BE value for *h*-BN/ NiCu_4 is equal to -0.18 eV *per* BN unit, which is between BEs for Ni and Cu.

DFT calculations indicate that the freestanding *h*-BN has a wide

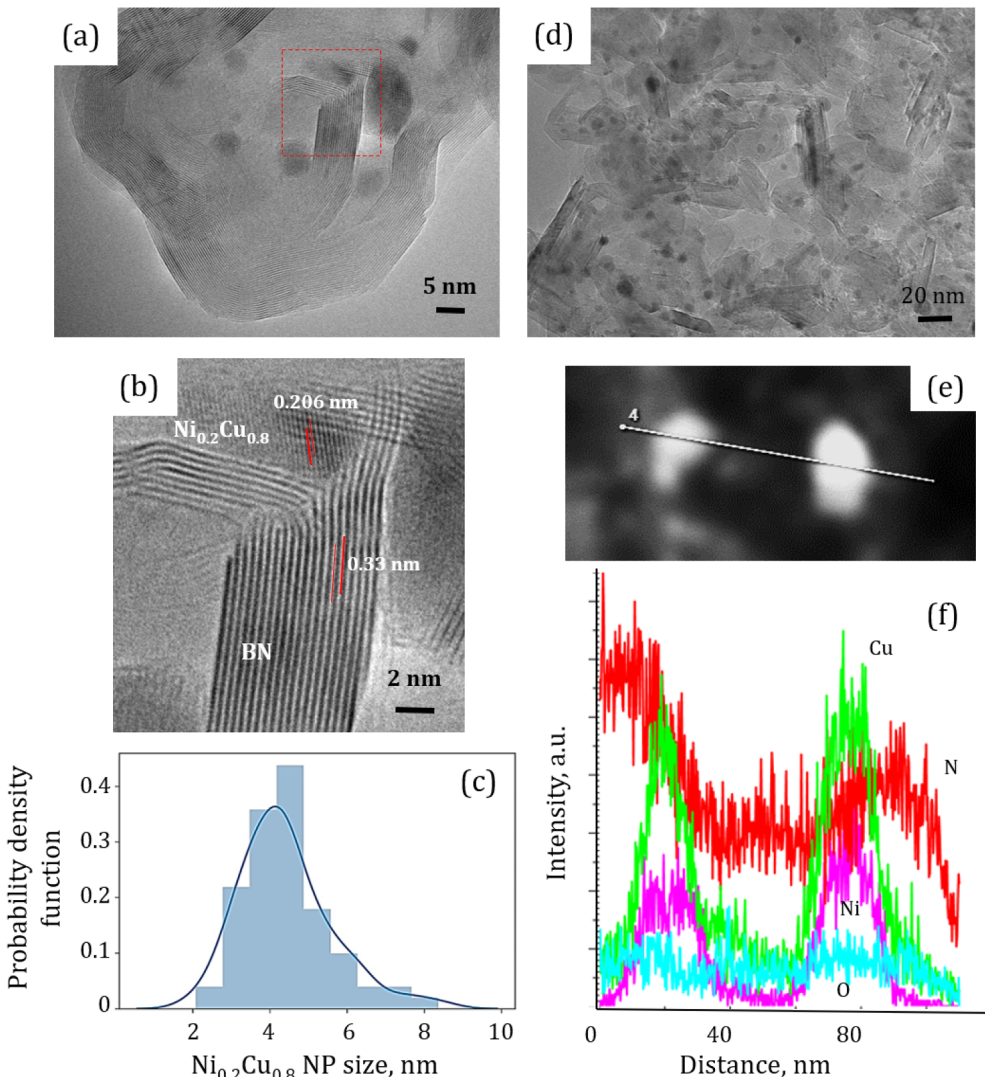


Fig. 5. TEM images of $(\text{Ni}_{0.2}\text{Cu}_{0.8})/\text{BN}$ nanohybrids before (a,b) and after (d) catalytic tests. $\text{Ni}_{0.2}\text{Cu}_{0.8}$ NP size distribution (c). STEM image (e) and corresponding EDX spectroscopy profiles (f) obtained from metallic nanoparticles after the catalytic test.

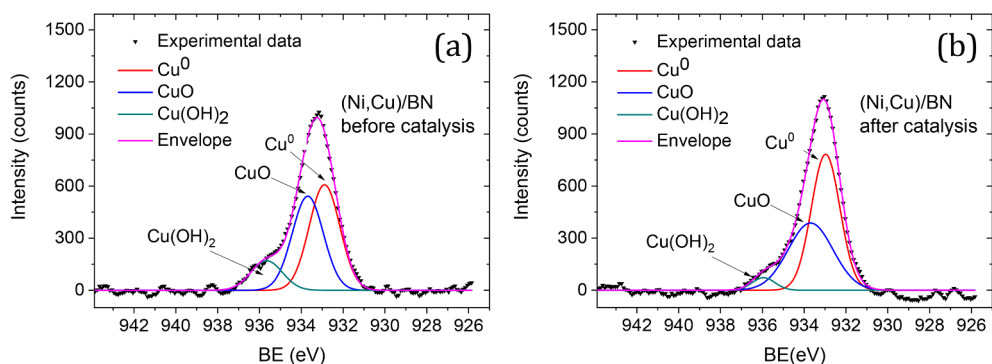


Fig. 6. XPS Cu 2p3/2 spectra and their curve fitting for (Ni_{0.2}Cu_{0.8})/BN nanohybrids before (a) and after (b) catalysis.

Table 4

Fractions (%) of different copper environments as derived from XPS Cu2p 3/2 curve fitting.

Sample	Cu ⁰ (BE = 932.9 eV, FWHM = 1.7 ± 0.05 eV)	CuO (BE = 933.7 eV, FWHM = 1.8 ± 0.05 eV)	Cu(OH) ₂ (BE = 935.6 eV, FWHM = 1.8 ± 0.05 eV)
(Ni _{0.2} Cu _{0.8})/BN before catalytic tests	45.6	41.3	13.1
(Ni _{0.2} Cu _{0.8})/BN after catalytic tests	54.2	41.8	4.0

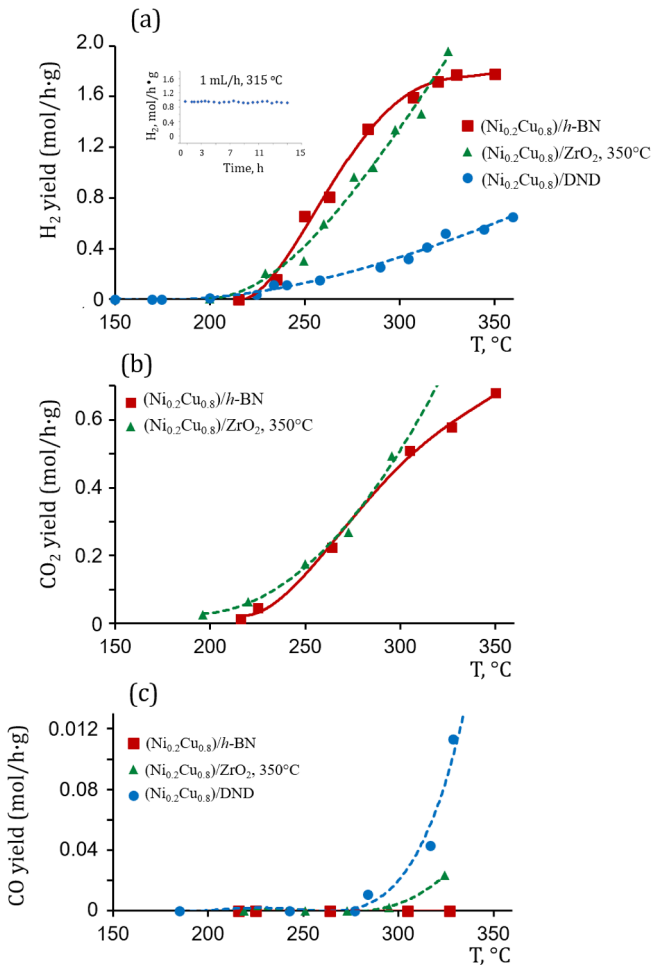


Fig. 7. Catalytic activities of various hybrid materials in the methanol steam reforming reaction. Temperature dependences of H₂ (a), CO₂ (b), and CO (c) yields in methanol steam reforming. (Ni_{0.2}Cu_{0.8})/h-BN – present study, (Ni_{0.2}Cu_{0.8})/ZrO₂, 350 °C [24], and (Ni_{0.2}Cu_{0.8})/DND [31].

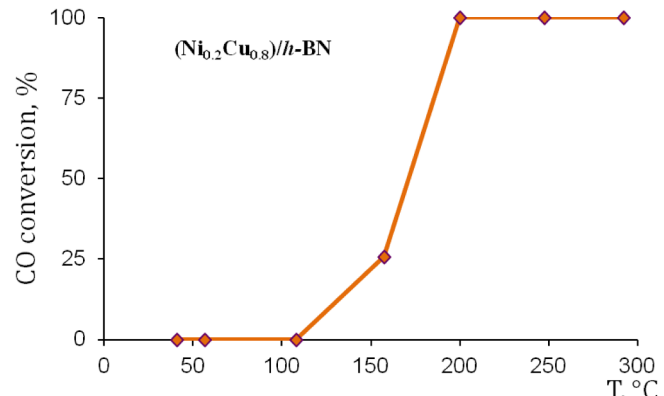


Fig. 8. Catalytic activities of (Ni_{0.2}Cu_{0.8})/h-BN nanohybrids in the CO oxidation reaction.

band gap of 4.5 eV, while for the *h*-BN-supported NiCu₄ (1 1 1), there are gap states above and below the Fermi level (Fig. 9b). Similar gap states were experimentally observed in *h*-BN-supported Ni and Rh metals [77]. The maximum value of CO sorption energy at the NiCu_x/*h*-BN interface is equal to -0.206 eV per molecule, which is two times higher in comparison with pure *h*-BN, which has sorption energy in the range of -99 to -46 meV. The high sorption energy value should allow the CO molecule to remain on the surface under temperature fluctuations, but not impede its diffusion toward catalytic center. At the same time, the maximum sorption energy of CO molecule on the pure metal surface is relatively high: -2.461 (Ni_(1 0 0)), -1.089 (Cu_(1 0 0)) and -2.049 eV (NiCu₄ alloy), thereby indicating that CO molecule would strongly bond with the metal surface. Note that these values are obtained for the case when CO molecule interacts with the metal surface via a carbon atom. In view of such large sorption energy values for pure metallic catalysts, the interaction of CO molecules with atomic oxygen during methanol conversion is unlikely. Importantly, DFT calculations clearly indicate the enhanced CO sorption energy on the NiCu_x/*h*-BN heterostructure when compared with pure *h*-BN due to charge redistribution in the BN layer. The formation of gap states around the Fermi level should promote CO oxidation by oxygen species, as suggested above.

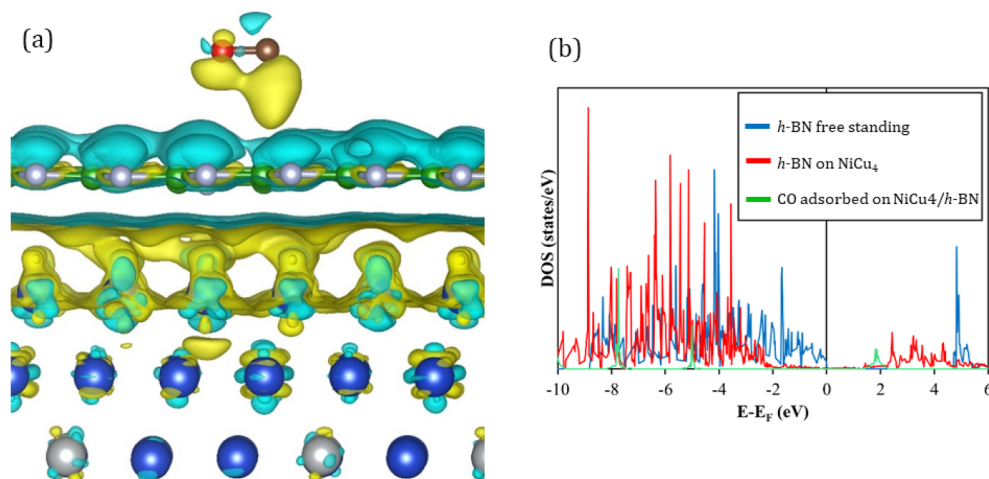


Fig. 9. Charge distribution in a CO-adsorbed NiCu₄/h-BN structure (a). Atom designations: Cu – large silver, Ni – blue, B – green, N – small silver, C – brown, and O – red. The isosurface level is $1.5 \times 10^{-4} \text{ e}/\text{\AA}^3$; positive and negative values are marked by yellow and cyan colors, respectively. Density of states for pure h-BN, NiCu₄/h-BN, and CO-adsorbed NiCu₄/h-BN (b). (For interpretation of the references to colour in this figure legend, the reader is referred to the web version of this article.)

5. Conclusions

(Ni_{0.2}Cu_{0.8})/BN nanohybrids with enhanced catalytic activity toward methanol steam reforming and CO oxidation have been obtained using a combination of boron oxide-assisted CVD method, vacuum annealing at 1500 °C for 1 h and reduction from salt solutions. The (Ni_{0.2}Cu_{0.8})/BN nanohybrids consist of h-BN nanosheets, 10–20 nm in lateral size, decorated with metallic nanoparticles, 3.0–8.2 nm in size. Most of the metallic NPs have kept their size below 10 nm after catalytic tests. The methanol dehydrogenation reaction starts at ~220 °C and is almost completed at 320 °C. The (Ni_{0.2}Cu_{0.8})/BN nanohybrids exhibit high catalytic stability and high selectivity for CO₂ over the whole temperature range. No carbon monoxide is detected. The onset temperature of catalytic CO oxidation is 100 °C and a full conversion is observed at 200 °C. DFT calculations show enhanced CO sorption energy on the h-BN/NiCu₄ heterostructure compared with pure h-BN due to charge redistribution in the BN layer. The formation of gap states around the Fermi level promotes CO oxidation by oxygen species.

Declaration of Competing Interest

The authors declare that they have no known competing financial interests or personal relationships that could have appeared to influence the work reported in this paper.

Acknowledgements

The authors gratefully acknowledge the financial support from the Ministry of Education and Science of the Russian Federation (Increase Competitiveness Program of NUST «MISiS» No. K2-2017-082) in the part of catalysis, and the Russian Foundation for Basic Research (Agreement 18-58-53034/19) in the part of DFT calculations. A.V.B. acknowledges the support from the Ministry of Education, Youth and Sports project “Novel nanostructures for engineering applications” No. CZ.02.1.01/0.0/0.0/16_026/0008396 and CzechNanoLab Research Infrastructure supported by MEYS CR (LM2018110). D.G. is grateful to the Australian Research Council (ARC) for granting a Laureate Fellowship No. FL160100089, QUT Project No. 323000-0355/51, and QUT Centre for Materials Science.

References

- [1] J.W. Patrick, Handbook of Fuel Cells. Fundamentals Technology and Applications, Wiley, Chichester, England, 2003 <https://doi.org/10.1016/j.fuel.2003.09.012>.
- [2] E. Gerasimova, E. Safranova, A. Ukshe, Y. Dobrovolsky, A. Yaroslavtsev, Electrocatalytic and transport properties of hybrid Nafion® membranes doped with silica and cesium acid salt of phosphotungstic acid in hydrogen fuel cells, Chem. Eng. J. 305 (2016) 121–128, <https://doi.org/10.1016/j.cej.2015.11.079>.
- [3] L. Carrette, K.A. Friedrich, U. Stimming, Fuel cells - fundamentals and applications, Fuel Cells. 1 (2001) 5–39, [https://doi.org/10.1002/1615-6854\(200105\)1:1<5::aid-fuce5>3.0.co;2-g](https://doi.org/10.1002/1615-6854(200105)1:1<5::aid-fuce5>3.0.co;2-g).
- [4] A.S. Aricò, S. Srinivasan, V. Antonucci, DMFCs: from fundamental aspects to technology development, Fuel Cells 1 (2001) 133–161, [https://doi.org/10.1002/1615-6854\(200107\)1:2<133::aid-fuce133>3.3.co;2-x](https://doi.org/10.1002/1615-6854(200107)1:2<133::aid-fuce133>3.3.co;2-x).
- [5] M.V. Tsodikov, A.V. Chistyakov, F.A. Yandieva, V.V. Zhmakin, A.E. Gekhman, I.I. Moiseev, Conversion of biomass products to energy sources in the presence of nanocatalysts and membrane-catalyst systems, Catal. Ind. 3 (2011) 4–10, <https://doi.org/10.1134/S2070050411010156>.
- [6] N.L. Basov, M.M. Ermilova, N.V. Orekhova, I.A. Oreshkin, A.B. Yaroslavtsev, Low temperature methane coupling in a Pd-based membrane reactor with UV activation, Mendeleev Commun. 23 (2013) 69–70, <https://doi.org/10.1016/j.mencom.2013.03.003>.
- [7] A. Heinzel, B. Vogel, P. Hübner, Reforming of natural gas - hydrogen generation for small scale stationary fuel cell systems, J. Power Sources 105 (2002) 202–207, [https://doi.org/10.1016/S0378-7753\(01\)00940-5](https://doi.org/10.1016/S0378-7753(01)00940-5).
- [8] Y. Shirasaki, T. Tsuneki, Y. Ota, I. Yasuda, S. Tachibana, H. Nakajima, K. Kobayashi, Development of membrane reformer system for highly efficient hydrogen production from natural gas, Int. J. Hydrogen Energy 34 (2009) 4482–4487, <https://doi.org/10.1016/j.ijhydene.2008.08.056>.
- [9] P. Durán, A. Sanz-Martínez, J. Soler, M. Menéndez, J. Herguido, Pure hydrogen from biogas: intensified methane dry reforming in a two-zone fluidized bed reactor using permselective membranes, Chem. Eng. J. 370 (2019) 772–781, <https://doi.org/10.1016/j.cej.2019.03.199>.
- [10] V.L. Kozhevnikov, I.A. Leonidov, M.V. Patrakeev, A.A. Markov, Y.N. Blinovskov, Evaluation of La_{0.55}Sr_{0.5}FeO_{3-δ} membrane reactors for partial oxidation of methane, J. Solid State Electrochem. 13 (2009) 391–395, <https://doi.org/10.1007/s10008-008-0572-9>.
- [11] A.A. Markov, O.A. Savinskaya, M.V. Patrakeev, A.P. Nemudry, I.A. Leonidov, Y.T. Pavlyukhin, A.V. Ishchenko, V.L. Kozhevnikov, Structural features, non-stoichiometry and high-temperature transport in SrFe_{1-x}Mo_xO_{3-δ}, J. Solid State Chem. 182 (2009) 799–806, <https://doi.org/10.1016/j.jssc.2008.12.026>.
- [12] Z. Gong, L. Hong, Integration of air separation and partial oxidation of methane in the La_{0.4}Ba_{0.6}Fe_{0.8}Zn_{0.2}O_{3-δ} membrane reactor, J. Membr. Sci. 380 (2011) 81–86, <https://doi.org/10.1016/j.memsci.2011.06.033>.
- [13] V.L. Kozhevnikov, I.A. Leonidov, M.V. Patrakeev, Ceramic membranes with mixed conductivity and their application, Russ. Chem. Rev. 82 (2013) 772–782, <https://doi.org/10.1070/rcc2013v08n08abeh004397>.
- [14] A.A. Markov, M.V. Patrakeev, I.A. Leonidov, V.L. Kozhevnikov, Reaction control and long-term stability of partial methane oxidation over an oxygen membrane, J. Solid State Electrochem. 15 (2011) 253–257, <https://doi.org/10.1007/s10008-010-1113-x>.
- [15] O.G. Ellert, M.V. Tsodikov, S.A. Nikolaev, V.M. Novotortsev, Bimetallic nanoalloys in heterogeneous catalysis of industrially important reactions: synergistic effects and structural organization of active components, Russ. Chem. Rev. 83 (2014) 718–732, <https://doi.org/10.1070/rcc2014v08n08abeh004432>.
- [16] L.L. Makarshin, V.N. Parmon, Microchannel catalytic systems for hydrogen energetics, Russ. J. Gen. Chem. 77 (2007) 676–684, <https://doi.org/10.1134/S1070363207040305>.
- [17] E.Y. Mironova, M.M. Ermilova, N.V. Orekhova, D.N. Muraviev, A.B. Yaroslavtsev, Production of high purity hydrogen by ethanol steam reforming in membrane reactor, Catal. Today 236 (2014) 64–69, <https://doi.org/10.1016/j.cattod.2014.01.014>.
- [18] A. Iulianelli, P. Ribeirinha, A. Mendes, A. Basile, Methanol steam reforming for hydrogen generation via conventional and membrane reactors: a review, Renew. Sustain. Energy Rev. 29 (2014) 355–368, <https://doi.org/10.1016/j.rser.2013.08.032>.
- [19] A.B. Yaroslavtsev, I.A. Stenina, T.L. Kulova, A.M. Skundin, A.V. Desyatov, Nanomaterials for electrical energy storage, Compr. Nanosci. Nanotechnol. 5 (2019) 165–206, <https://doi.org/10.1016/b978-0-12-803581-8.10426-6>.

- [20] A.A. Lytkina, N.V. Orekhova, A.B. Yaroslavtsev, Catalysts for the steam reforming and electrochemical oxidation of methanol, Inorg. Mater. 54 (2018) 1315–1329, <https://doi.org/10.1134/S0020168518130034>.
- [21] R. Pérez-Hernández, G. Mondragón Galicia, D. Mendoza Anaya, J. Palacios, C. Angeles-Chavez, J. Arenas-Alatorre, Synthesis and characterization of bimetallic Cu-Ni/ZrO₂ nanocatalysts: H₂ production by oxidative steam reforming of methanol, Int. J. Hydrogen Energy 33 (2008) 4569–4576, <https://doi.org/10.1016/j.ijhydene.2008.06.019>.
- [22] P. Tahay, Y. Khani, M. Jabari, F. Bahadoran, N. Safari, Highly porous monolith/TiO₂ supported Cu, Cu-Ni, Ru, and Pt catalysts in methanol steam reforming process for H₂ generation, Appl. Catal. A Gen. 554 (2018) 44–53, <https://doi.org/10.1016/j.apcata.2018.01.022>.
- [23] R. Pérez-Hernández, A. Gutiérrez-Martínez, M.E. Espinosa-Pesqueira, M.L. Estanislao, J. Palacios, Effect of the bimetallic Ni/Cu loading on the ZrO₂ support for H₂ production in the autothermal steam reforming of methanol, Catal. Today 250 (2015) 166–172, <https://doi.org/10.1016/j.cattod.2014.08.009>.
- [24] A.A. Lytkina, N.V. Orekhova, M.M. Ermilova, A.B. Yaroslavtsev, The influence of the support composition and structure (MXZr_{1-x}O_{2-x}) of bimetallic catalysts on the activity in methanol steam reforming, Int. J. Hydrogen Energy 43 (2018) 198–207, <https://doi.org/10.1016/j.ijhydene.2017.10.182>.
- [25] Y. Khani, F. Bahadoran, S. Soltanali, J.S. Ahari, Hydrogen production by methanol steam reforming on a cordierite monolith reactor coated with Cu-Ni/LaZnAlO₄ and Cu-Ni/γ-Al₂O₃ catalysts, Res. Chem. Intermed. 44 (2018) 925–942, <https://doi.org/10.1007/s11164-017-3144-8>.
- [26] M. Khzouz, E.I. Gkanas, S. Du, J. Wood, Catalytic performance of Ni-Cu/Al₂O₃ for effective syngas production by methanol steam reforming, Fuel 232 (2018) 672–683, <https://doi.org/10.1016/j.fuel.2018.06.025>.
- [27] T. Saeki, K. Tsuda, H. Ohkita, N. Kakuta, T. Mizushima, Compositional effects of ceria-supported nickel-copper catalyst on its reduction behavior and catalytic performance for ethanol steam reforming, J. Japan Pet. Inst. 59 (2016) 16–23, <https://doi.org/10.1627/jpi.59.16>.
- [28] L.C. Chen, S.D. Lin, Effects of the pretreatment of CuNi/SiO₂ on ethanol steam reforming: Influence of bimetal morphology, Appl. Catal. B Environ. 148–149 (2014) 509–519, <https://doi.org/10.1016/j.apcatb.2013.11.031>.
- [29] T. Wu, Q. Zhang, W. Cai, P. Zhang, X. Song, Z. Sun, L. Gao, Phyllosilicate evolved hierarchical Ni- and Cu-Ni/SiO₂ nanocomposites for methane dry reforming catalysis, Appl. Catal. A Gen. 503 (2015) 94–102, <https://doi.org/10.1016/j.apcata.2015.07.012>.
- [30] A. Carrero, J.A. Calles, A.J. Vizcaíno, Effect of Mg and Ca addition on coke deposition over Cu-Ni/SiO₂ catalysts for ethanol steam reforming, Chem. Eng. J. 163 (2010) 395–402, <https://doi.org/10.1016/j.cej.2010.07.029>.
- [31] E.Y. Mironova, A.A. Lytkina, M.M. Ermilova, M.N. Efimov, L.M. Zemtsov, N.V. Orekhova, G.P. Karpareva, G.N. Bondarenko, D.N. Muraviev, A.B. Yaroslavtsev, Ethanol and methanol steam reforming on transition metal catalysts supported on detonation synthesis nanodiamonds for hydrogen production, Int. J. Hydrogen Energy 40 (2015) 3557–3565, <https://doi.org/10.1016/j.ijhydene.2014.11.082>.
- [32] A.A. Lytkina, N.V. Orekhova, M.M. Ermilova, I.S. Petriev, M.G. Baryshev, A.B. Yaroslavtsev, Ru-Rh based catalysts for hydrogen production via methanol steam reforming in conventional and membrane reactors, Int. J. Hydrogen Energy 44 (2019) 13310–13322, <https://doi.org/10.1016/j.ijhydene.2019.03.205>.
- [33] M.A. Newton, D. Ferri, G. Smolentsev, V. Marchionni, M. Nachtegaal, Room-temperature carbon monoxide oxidation by oxygen over Pt/Al₂O₃ mediated by reactive platinum carbonates, Nat. Commun. 6 (2015) 8675, <https://doi.org/10.1038/ncomms9675>.
- [34] A. Mishra, R. Prasad, A review on preferential oxidation of carbon monoxide in hydrogen rich gases, Bull. Chem. React. Eng. Catal. 6 (2011) 1–14, <https://doi.org/10.9767/bcrec.6.1.191.1-14>.
- [35] N.K. Soliman, Factors affecting CO oxidation reaction over nanosized materials: a review, J. Mater. Res. Technol. 8 (2019) 2395–2407, <https://doi.org/10.1016/j.jmrt.2018.12.012>.
- [36] R.M. Al Soubaihi, K.M. Saoud, J. Dutta, Critical review of low-temperature CO oxidation and hysteresis phenomenon on heterogeneous catalysts, Catalysts 8 (2018) 660, <https://doi.org/10.3390/catal8120660>.
- [37] A. Biabani-Ravandi, M. Rezaei, Z. Fattah, Study of Fe-Co mixed metal oxide nanoparticles in the catalytic low-temperature CO oxidation, Process Saf. Environ. Prot. 91 (2013) 489–494, <https://doi.org/10.1016/j.psep.2012.10.015>.
- [38] J.T. Grant, C.A. Carrero, F. Goeltl, J. Venegas, P. Mueller, S.P. Burt, S.E. Specht, W.P. McDermott, A. Chieregato, I. Hermans, Selective oxidative dehydrogenation of propane to propene using boron nitride catalysts, Science 354 (2016) 1570–1573, <https://doi.org/10.1126/science.aaf7885>.
- [39] R. Huang, B. Zhang, J. Wang, K.-H. Wu, W. Shi, Y. Zhang, Y. Liu, A. Zheng, R. Schlögl, D.S. Su, Direct insight into ethane oxidative dehydrogenation over boron nitrides, ChemCatChem 9 (2017) 3293–3297, <https://doi.org/10.1002/cctc.201700725>.
- [40] L. Wang, C. Sun, L. Xu, Y. Qian, Convenient synthesis and applications of gram scale boron nitride nanosheets, Catal. Sci. Technol. 1 (2011) 1119–1123, <https://doi.org/10.1039/c1cy00191d>.
- [41] H. Zhao, J. Song, X. Song, Z. Yan, H. Zeng, Ag/white graphene foam for catalytic oxidation of methanol with high efficiency and stability, J. Mater. Chem. A 3 (2015) 6679–6684, <https://doi.org/10.1039/c4ta07053d>.
- [42] A. Lyalin, A. Nakayama, K. Uosaki, T. Taketsugu, Adsorption and catalytic activation of the molecular oxygen on the metal supported h-BN, Top. Catal. 57 (2014) 1032–1041, <https://doi.org/10.1007/s11244-014-0267-7>.
- [43] K. Uosaki, G. Elumalai, H. Noguchi, T. Masuda, A. Lyalin, A. Nakayama, T. Taketsugu, Boron nitride nanosheet on gold as an electrocatalyst for oxygen reduction reaction: theoretical suggestion and experimental proof, J. Am. Chem. Soc. 136 (2014) 6542–6545, <https://doi.org/10.1021/ja500393g>.
- [44] Y. Zhou, Y. Wang, T. Liu, G. Xu, G. Chen, H. Li, L. Liu, Q. Zhuo, J. Zhang, C. Yan, Superhydrophobic h-BN-regulated sponges with excellent absorbency fabricated using a green and facile method, Sci. Rep. 7 (2017) 45065, <https://doi.org/10.1038/srep45065>.
- [45] X. Liu, T. Duan, Y. Sui, C. Meng, Y. Han, Copper atoms embedded in hexagonal boron nitride as potential catalysts for CO oxidation: a first-principles investigation, RSC Adv. 4 (2014) 38750–38760, <https://doi.org/10.1039/C4RA06436D>.
- [46] A.M. Kovalskii, A.T. Matveev, O.I. Lebedev, I.V. Sukhorukova, K.L. Firestein, A.E. Steinman, D.V. Shtansky, D. Golberg, Growth of spherical boron oxynitride nanoparticles with smooth and petalled surfaces during a chemical vapour deposition process, CrystEngComm 18 (2016) 6689–6699, <https://doi.org/10.1039/c6ce01126h>.
- [47] A.S. Konopatsky, K.L. Firestein, D.V. Leybo, Z.I. Popov, K.V. Larionov, A.E. Steinman, A.M. Kovalskii, A.T. Matveev, A.M. Manakhov, P.B. Sorokin, D. Golberg, D.V. Shtansky, BN nanoparticle/Ag hybrids with enhanced catalytic activity: theory and experiments, Catal. Sci. Technol. 8 (2018) 1652–1662, <https://doi.org/10.1039/c7cy02207g>.
- [48] K.L. Firestein, D.V. Leybo, A.E. Steinman, A.M. Kovalskii, A.T. Matveev, A.M. Manakhov, I.V. Sukhorukova, P.V. Slukin, N.K. Fursova, S.G. Ignatov, D.V. Golberg, D.V. Shtansky, BN/Ag hybrid nanomaterials with petal-like surfaces as catalysts and antibacterial agents, Beilstein J. Nanotechnol. 9 (2018) 250–261, <https://doi.org/10.3762/bjnano.9.27>.
- [49] A. Manakhov, P. Kiryukhantsev-Korneev, M. Michlíček, E. Permyakova, E. Dvořáková, J. Polcák, Z. Popov, M. Visotin, D.V. Shtansky, Grafting of carboxyl groups using CO₂/C₂H₄/Ar pulsed plasma: theoretical modeling and XPS derivation, Appl. Surf. Sci. 435 (2018) 1220–1227, <https://doi.org/10.1016/j.apsusc.2017.11.174>.
- [50] A. Manakhov, M. Michlíček, A. Felten, J.J. Pireaux, D. Nečas, L. Zajíčková, XPS depth profiling of derivatized amine and anhydride plasma polymers: evidence of limitations of the derivatization approach, Appl. Surf. Sci. 394 (2017) 578–585, <https://doi.org/10.1016/j.apsusc.2016.10.099>.
- [51] P. Hohenberg, W. Kohn, Inhomogeneous electron gas, Phys. Rev. 136 (1964) B864, <https://doi.org/10.1103/PhysRev.136.B864>.
- [52] W. Kohn, L.J. Sham, Self-consistent equations including exchange and correlation effects, Phys. Rev. 140 (1965) A1133, <https://doi.org/10.1103/PhysRev.140.A1133>.
- [53] J.P. Perdew, K. Burke, M. Ernzerhof, Generalized gradient approximation made simple, Phys. Rev. Lett. 77 (1996) 3865–3868, <https://doi.org/10.1103/PhysRevLett.77.3865>.
- [54] P.E. Blöchl, Projector augmented-wave method, Phys. Rev. B. 50 (1994) 17953–17979, <https://doi.org/10.1103/PhysRevB.50.17953>.
- [55] H.J. Monkhorst, J.D. Pack, Special points for Brillouin-zone integrations, Phys. Rev. B. 13 (1976) 5188–5192, <https://doi.org/10.1103/PhysRevB.13.5188>.
- [56] S. Grimme, J. Antony, S. Ehrlich, H. Krieg, A consistent and accurate ab initio parametrization of density functional dispersion correction (DFT-D) for the 94 elements H-Pu, J. Chem. Phys. 132 (2010) 154104, , <https://doi.org/10.1063/1.3382344>.
- [57] O.M. Moon, B.C. Kang, S.B. Lee, J.H. Boo, Temperature effect on structural properties of boron oxide thin films deposited by MOCVD method, Thin Solid Films 464–465 (2004) 164–169, <https://doi.org/10.1016/j.tsf.2004.05.107>.
- [58] Z.F. Ying, D. Yu, H. Ling, N. Xu, Y.F. Lu, J. Sun, J.D. Wu, Synthesis of BCN thin films by nitrogen ion beam assisted pulsed laser deposition from a B₄C target, Diam. Relat. Mater. 16 (2007) 1579–1585, <https://doi.org/10.1016/j.diamond.2007.01.021>.
- [59] A.R. Naghash, T.H. Etsell, S. Xu, XRD and XPS study of Cu–Ni interactions on reduced copper–nickel–aluminum oxide solid solution catalysts, Chem. Mater. 18 (10) (2006) 2480–2488, <https://doi.org/10.1021/cm051910a>.
- [60] I. Zegkinoglou, L. Pielsticker, Z.-K. Han, N.J. Divins, D. Kordus, Y.-T. Chen, C. Escudero, V. Perez-Dieste, B. Zhu, Y. Gao, B.R. Cuanya, Surface segregation in CuNi nanoparticle catalysts during CO₂ hydrogenation: the role of CO in the reactant mixture, J. Phys. Chem. C 123 (2019) 8421–8428, <https://doi.org/10.1021/acs.jpcc.8b09912>.
- [61] M.C. Biesinger, Advanced analysis of copper X-ray photoelectron spectra, Surf. Interface Anal. 49 (2017) 1325–1334, <https://doi.org/10.1002/sia.6239>.
- [62] J.P. Espinós, J. Morales, A. Barranco, A. Caballero, J.P. Holgado, A.R. González-Elípe, Interface effects for Cu, Cu₂O, and Cu₂O deposited on SiO₂ and ZrO₂, XPS determination of the valence state of copper in Cu/SiO₂ and Cu/ZrO₂ catalysts, Phys. Chem. B 106 (2002) 6921–6929, <https://doi.org/10.1021/jp014618m>.
- [63] A.S. Konopatsky, D.V. Leybo, K.L. Firestein, Z.I. Popov, A.V. Bondarev, A.M. Manakhov, E.S. Permyakova, D.V. Shtansky, D.V. Golberg, Synthetic routes, structure and catalytic activity of Ag/BN nanoparticle hybrids toward CO oxidation reaction, J. Catal. 368 (2018) 217–227, <https://doi.org/10.1016/j.jcat.2018.10.016>.
- [64] K. Takahashi, N. Takezawa, H. Kobayashi, The mechanism of steam reforming of methanol over a copper-silica catalyst, Appl. Catal. 2 (1982) 363–366, [https://doi.org/10.1016/0166-9834\(82\)80154-1](https://doi.org/10.1016/0166-9834(82)80154-1).
- [65] C.J. Jiang, D.L. Trimm, M.S. Wainwright, N.W. Cant, Kinetic study of steam reforming of methanol over copper-based catalysts, Appl. Catal. A 93 (1993) 245–255, [https://doi.org/10.1016/0926-860X\(93\)85197-W](https://doi.org/10.1016/0926-860X(93)85197-W).
- [66] J.P. Breen, J.R.H. Ross, Methanol reforming for fuel-cell applications: development of zirconia-containing Cu-Zn-Al catalysts, Catal. Today 51 (1999) 521–533, [https://doi.org/10.1016/S0920-5861\(99\)00038-3](https://doi.org/10.1016/S0920-5861(99)00038-3).
- [67] N. Takezawa, N. Iwasa, Steam reforming and dehydrogenation of methanol: difference in the catalytic functions of copper and group VIII metals, Catal. Today 36

- (1997) 45–56, [https://doi.org/10.1016/S0920-5861\(96\)00195-2](https://doi.org/10.1016/S0920-5861(96)00195-2).
- [68] T. Shishido, Y. Yamamoto, H. Morioka, K. Takehira, Production of hydrogen from methanol over Cu/ZnO and Cu/ZnO/Al₂O₃ catalysts prepared by homogeneous precipitation: steam reforming and oxidative steam reforming, *J. Mol. Catal. A Chem.* 268 (2007) 185–194, <https://doi.org/10.1016/j.molcata.2006.12.018>.
- [69] J.C. Amplett, M.J. Evans, R.F. Mann, R.D. Weir, Hydrogen production by the catalytic steam reforming of methanol: Part 2: kinetics of methanol decomposition using girdler G66B catalyst, *Can. J. Chem. Eng.* 63 (1985) 605–611, <https://doi.org/10.1002/cjce.5450630412>.
- [70] A.H.M.A. Wasey, S. Chakrabarty, G.P. Das, C. Majumder, h-BN monolayer on the Ni (111) surface: a potential catalyst for oxidation, *ACS Appl. Mater. Interfaces* 5 (2013) 10404–10408, <https://doi.org/10.1021/am404321x>.
- [71] S. Lin, J. Huang, X. Gao, A Cu(111) supported h-BN nanosheet: a potential low-cost and high-performance catalyst for CO oxidation, *Phys. Chem. Chem. Phys.* 17 (2015) 22097–22105, <https://doi.org/10.1039/c5cp03027g>.
- [72] R. Laskowski, P. Blaha, K. Schwarz, Bonding of hexagonal BN to transition metal surfaces: an ab initio density-functional theory study, *Phys. Rev. B* 78 (2008) 045409, , <https://doi.org/10.1103/PhysRevB.78.045409>.
- [73] J. Gómez Díaz, Y. Ding, R. Koitz, A.P. Seitsonen, M. Iannuzzi, J. Hutter, Hexagonal boron nitride on transition metal surfaces, *Theor. Chem. Acc.* 132 (2013) 1–17, <https://doi.org/10.1007/s00214-013-1350-z>.
- [74] G. Hu, Z. Wu, S. Dai, D.E. Jiang, Interface engineering of earth-abundant transition metals using boron nitride for selective electroreduction of CO₂, *ACS Appl. Mater. Interfaces* 10 (2018) 6694–6700, <https://doi.org/10.1021/acsami.7b17600>.
- [75] A.B. Preobrajenski, A.S. Vinogradov, N. Mårtensson, Ni 3d–BN π hybridization at the h–BN/Ni(111) interface observed with core-level spectroscopies, *Phys. Rev. B* 70 (2004) 165404, , <https://doi.org/10.1103/PhysRevB.70.165404>.
- [76] A.B. Preobrajenski, A.S. Vinogradov, N. Mårtensson, Monolayer of h-BN chemisorbed on Cu(111) and Ni(111): the role of the transition metal 3d states, *Surf. Sci.* 582 (2005) 21–30, <https://doi.org/10.1016/j.susc.2005.02.047>.
- [77] A.B. Preobrajenski, S.A. Krasnikov, A.S. Vinogradov, M.L. Ng, T. Käämbe, A.A. Cafolla, N. Mårtensson, Adsorption-induced gap states of h-BN on metal surfaces, *Phys. Rev. B* 77 (2008) 085421, , <https://doi.org/10.1103/PhysRevB.77.085421>.